Corrosion Science 167 (2020) 108511

Contents lists available at ScienceDirect

Corrosion Science

journal homepage: www.elsevier.com/locate/corsci

Continuous KCl addition in high temperature exposures of 304 L – A way to mimic a boiler environment

J. Phother-Simon*, T. Jonsson, J. Liske

Environmental Inorganic Chemistry, Department of Chemistry and Chemical Engineering, Chalmers University of Technology, S-412 96, Göteborg, Sweden

ARTICLE INFO

Keywords:
Oxidation
KCl
304 L
Deposits
High temperature corrosion

ABSTRACT

Alloys exposed in waste-fired boilers tend to exhibit higher corrosion rates and more signs of severe corrosion attack than in laboratory experiments simulating this type of environment. Thus, in order to better mimic the boiler environment, a laboratory setup with continuous deposition of KCl(s) on the samples has been performed. Areas with high amount of deposited KCl(s) reveal an accelerated corrosion attack characterized by thick oxide layers, void formation and steel grain boundary attack. Areas with less deposited KCl(s) exhibited the same morphology as presented earlier for 304 L samples exposed to small amount of KCl(s).

1. Introduction

The release of greenhouse gases (GHG) to the atmosphere due to human activities has steadily been increasing [1]. The majority of GHG are produced during the combustion of fossil fuels where carbon dioxide (CO_2) is a rest product. The release of GHGs to the atmosphere cause global warming and increasing efforts are now being put forward to reduce this trend. One way to reduce the net emission of CO_2 is the substitution of fossil fuels with renewable fuels in power plants. Unfortunately, the combustion of renewable fuels such as biomass and waste usually result in the formation of corrosive deposits and gases that damage critical parts of the plant. From a corrosion aspect, the resulting flue gas when combusting biomass and waste contains mainly water vapor, carbon dioxide, alkali chlorides and hydrogen chloride [2–8]. Consequently, the deposit formed on the superheater tubes are mainly constituted of alkali chlorides, which are known for their corrosiveness towards superheater tubes [2,7,9–21]. The corrosiveness of the alkali chlorides is explained by one of the following mechanisms: the “chromate formation” mechanism [2,12,13,16,10–21] where the alkali deteriorates the protective chromium-rich layer on stainless steels by the formation of alkali chromate and an iron rich non-protective scale, or, the “active oxidation” mechanism [7,11,22–27] where the $Cl_2(g)$ is transported through the oxide scale to the oxide/metal interface. Subsequently, the $Cl_2(g)$ reacts with the metal to form metal chlorides that diffuse as $MeCl_x(g)$ back through the oxide scale, cracks and pores, towards the gas/oxide interface. The higher partial pressure of oxygen at the gas/oxide interface leads to decomposition of $MeCl_x(g)$ into Me_xO_y, releasing $Cl_2(g)$ to the atmosphere. The released $Cl_2(g)$ can again be transported towards the metal/oxide interface, repeating the process in a cyclic manner. An electrochemical approach has also been suggested, which suggests that a flux of anions, cations and an electronic current occurs instead of a gas transport of chlorine through the oxide scale [28,29].

The laboratory studies investigating the corrosive effect of KCl at high temperatures are usually performed with a fixed amount of KCl(s) deposited on the samples *ex-situ* prior to exposure as in *e.g.* [30] or with a layer of KCl(s) that covers the sample [12,18]. However, this rather static manner of applying the salt does not resemble the deposit formation that occurs on *e.g.* superheater tubes in boilers. Furthermore, the corrosion attack and deposit formation occur simultaneously on field samples, probably affecting each other. For this reason, to better mimic the boiler environment and to study the propagation of the corrosion attack, a laboratory setup with continuous deposition of KCl (s) on the sample surface has been developed.

2. Theory – Aim of the method

The corrosive effect at high temperatures of alkali salts on materials used for superheater tubes has been investigated assiduously in laboratory studies [2,7,9–21,30–32]. For stainless steels at high temperatures (~ 600 °C) and in an oxidizing atmosphere, the morphology of the corrosion attacks can be characterized by an outward-growing iron oxide, an inward-growing spinel oxide and, depending on the amount of KCl present, grain boundary attacks. However, the corrosive effect of alkali salts has also been investigated in field studies in *e.g.* waste-fired boilers [2,33,34]. It can be observed that the severity of the

* Corresponding author.
E-mail address: julien.phother@chalmers.se (J. Phother-Simon).

https://doi.org/10.1016/j.corsci.2020.108511
Received 26 June 2019; Received in revised form 15 January 2020; Accepted 24 January 2020
Available online 30 January 2020
0010-938X/

corrosion attack is greater in waste-fired boilers than in laboratory exposures. Multi-layered oxides, thicker oxides, detachment of non-oxidized metal fragments as well as deeper grain boundary attacks are characteristic features observable on stainless steels exposed in waste-fired boilers. This shows the extensive divergence in corrosiveness between laboratory and field exposures. Thus, to unravel the severity of corrosion attacks that occur in waste-fired boilers, it is necessary to simulate an environment similar to waste-fired boilers. This can be attained by achieving a more corrosive environment in laboratory exposures.

Usually, the investigations of the corrosive effect of KCl at high temperatures are performed with fixed amounts of KCl(s) deposited on samples before exposure [30] or with a layer of KCl(s) that covers the sample [12,18]. However, this technique of investigating the effect of salt is mostly relevant for studies on the initiation of corrosion. When focusing on the propagation of corrosion attack (such as longer exposure durations), the initial supply of KCl may decrease or even become negligible which may not resemble the deposit formation that occurs in waste-fired boilers.

That is why, to replicate such environment, an experimental setup allowing continuous deposition of KCl onto the samples during exposure has been developed.

3. Materials and methods

3.1. Sample preparation

The material investigated is the austenitic steel 304 L from Outokumpu, the composition is given in the Table 1. The samples have the following dimensions: 15 × 15 × 2 mm^3 with a hole of 1.5 mm diameter drilled at 2 and 7.5 mm from the edges. All samples were grinded with 500 grit SiC from Struers and then polished with 9, 3, and 1 µm diamond solutions DP-Suspension using DP-Lubricant Yellow. As a final step, the samples were cleaned in acetone then ethanol using an ultrasonic bath Elmasonic P from Elma.

3.2. Exposures

The continuously deposited KCl exposures were performed in an atmosphere of 5 % O_2 + 20 % H_2O and balanced with N_2. The water vapor content was established by using the nafion membranes FC 125-240-5MP from Perma Pure. The flow rate was 2.5 cm/s and measured with a flowmeter Definer 220 from Bios. A 3-zone furnace ETF 80/12-III from Entech equipped with a 70-mm silica tube from Quarzglas Komponenten und Service QCS GmBH were used. An alumina boat filled with KCl(s) from VWR BDH Chemicals (assay 100.1 %) was placed upstream at 700 °C where the vapor pressure of KCl(s) calculated was 65.9 ppm, and the samples were placed downstream at 600 °C where the vapor pressure calculated was 3.4 ppm. Therefore, massive condensation of the salt in the samples area was expected during the exposure. The positions of the samples and the KCl boat were consistent for all exposures. The vapor pressures of KCl(s) at these two temperatures were calculated using the software FactSage 7.2 and the FTslat database. A schematic drawing of the setup is shown in Fig. 1. The duration of the exposures was based on previous work standards to make the comparison easier between the two methods. For this reason, the duration of the exposures was set to 24 h.

The temperature gradient profile within the furnace is shown in Fig. 2 and was measured twice to find the temperature variance between two experiments, as the furnace was turned off in between. The measurements were performed by moving a thermocouple forward every 1 cm from one side of the tube to the other side for a total length of 75 cm, see Fig. 3. The position of the thermocouple was consistently kept at the center of the furnace (co-axial), which means that the thermocouple was pushed forward while remaining aligned with the rotation axis of the tube.

The measurements were performed using two parallel gold foils, whose mass gains of KCl were measured discontinuously every 24 h for one week due to the deposition. Every 24 h, the two gold foils were taken out of the furnace and weight measured, while a set of two new gold foils were placed for the next 24 h. The measurements were performed for one week, which can be seen as seven sets of 24 -h exposure. Between each of those 24 -h exposure, the KCl(s) source was refilled. One of the gold foils is aligned with the rotation axis of the furnace (middle position) while the second gold foil is located at one of the sides, in order to replicate the position of future real samples at the same locations. The side positions are located 1.8 cm apart from the middle position and 1.5 cm apart from of the tube furnace, see Fig. 4.

In comparison, the previous way of applying salt consists in spraying or depositing KCl(s) onto the samples prior to exposure [13,16,30,35], which results in a limited amount of supplied KCl(s), such as 0.250 g deposited on top of the surface and 0.1 or 1.0 mg/cm^2 sprayed on the surface.

Table 1
Chemical composition of 304 L.

Element (wt.%)	Fe	Cr	Ni	Mn	Si
304 L	Bal.	20	10	1.4	< 0.6

4. Analytical techniques

Ion etching was used to obtain cross-sections with smooth surfaces for SEM imaging thanks to Broad Ion Beam (BIB) milling. This technique uses a triple ion beam cutter Leica TIC 3X, which uses argon ions for milling. The sessions were operated at 6.5 kV with a duration of 12 h. In order to prepare the sample for the BIB milling, a piece of silicon wafer was glued to the surface of the exposed sample using Loctite 415. After drying, the sample was cut in two pieces using a low speed saw Minitom from Struers. One of the two pieces could be subsequently inserted in the BIB.

The SEM imaging was performed using a FEI Quanta 200 ESEM FEG equipped with an Oxford Instruments X-Max^N 80 T EDX. The accelerating voltage used for imaging was 10 kV with 12 mm working distance, and 20 kV with 10 mm working distance for EDX analysis.

5. Results

5.1. Characteristics and observations of the novel laboratory setup

The temperature gradient profile within the furnace shown in Fig. 2 was measured twice and exhibits a consistent temperature profile in the area of interest. Only at the edges of the furnace (close to 0 cm and 75 cm on the X axis of the graph), a deviation between the two measurements was observed. This is due to the poor temperature control at the edges of the furnace. However, in the area of interest, located between 35 cm (samples position) and 55 cm (KCl source position), no relevant deviation was observed.

Due to the diameter of the tube and the laminar flow, a temperature spread of ± 2.5 °C was considered. This uncertainty was empirically confirmed by an average of measurements performed by shifting a thermocouple 1 cm in one direction, from the center, during the measurement of the profile temperature. The highest temperature was localized at the original measurement point, which was on the rotation axis of the tube, while the measurements performed by shifting the thermocouple 1 cm in one direction exhibited a lower temperature of maximum 2.5 °C, see Fig. 5.

The graph in the Fig. 6 shows the amount of KCl deposited on gold foils every 24 h for one week. Two positions of samples were investigated: middle of the furnace and the sides. As a reminder, the middle position is located at the center of the furnace while the sides

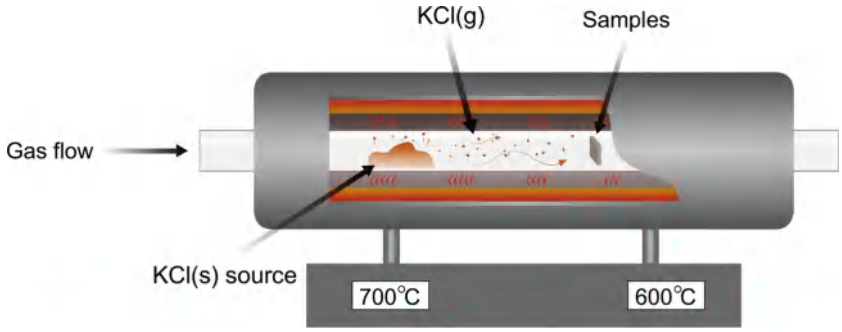

Fig. 1. Schematic drawing of the experimental setup.

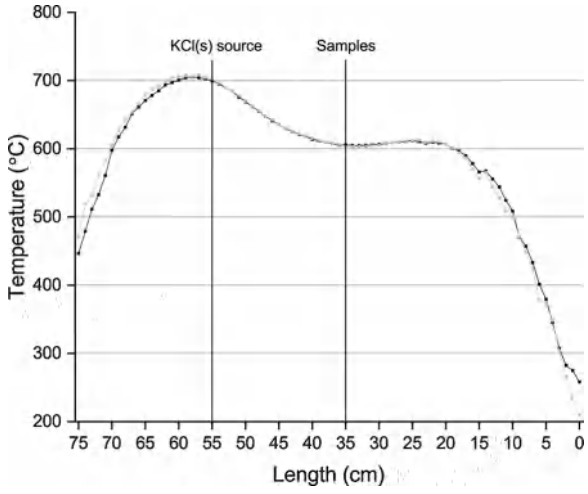

Fig. 2. Temperature profile for the 3-zone heating furnace measured twice with a shutdown in between.

positions are 1.8 cm apart from the center, and 1.5 cm from the walls. The position on the side averaged half the amount of KCl deposited at the middle position. Furthermore, the amount of KCl deposited every 24 h cycle during the one-week exposure remains relatively consistent: the average deposited amount of KCl was 0.95 mg/cm^2 per day ± 0.31 mg/cm^2 at the middle position, and 0.44 mg/cm^2 per day ± 0.11 mg/cm^2 at the side position.

In Fig. 7, a representative photograph of the exposed samples, directly after removal from the furnace is shown. The KCl deposits on the sample surface appear heterogeneous. The top of the samples exhibits more KCl deposition compared to the bottom part of the samples. Therefore, a gradient in the amount of KCl is observed on the samples from the top to the bottom. Moreover, the condensation of KCl between the samples is also heterogeneous. The middle sample exhibits substantial deposition/condensation and needle-like KCl particles can be seen on the sample surface. The sample to the left, which is a side sample, exhibits a lower KCl deposition/condensation. Consequently,

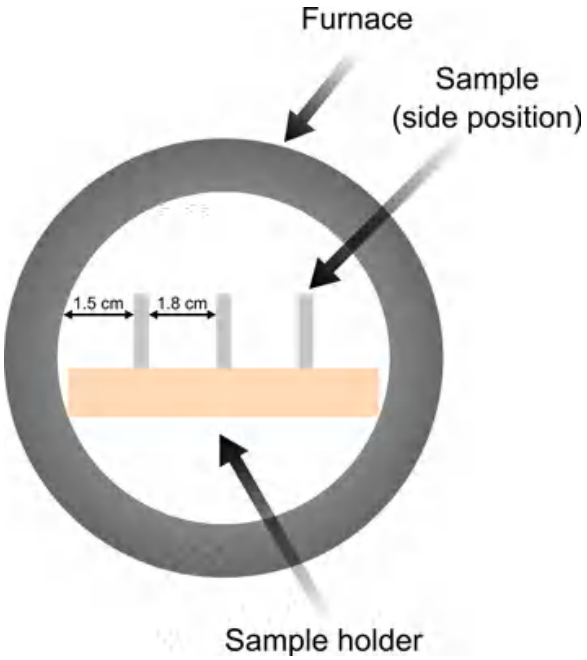

Fig. 4. Schematic drawing of the sample positions within the furnace in a cross-sectional view.

two areas were defined based on both, KCl deposition and different level of suspected corrosiveness: the top part of a middle sample is considered to be the most corroded area of the exposure (labelled “high amount of KCl”), while the bottom part of a side sample is the least corroded area (labelled “low amount of KCl”). Several exposures under the same conditions were performed and exhibited the same features.

Hence, as it was shown previously based on the measurement of KCl (s) deposition and the definition of different areas on the samples, that the setup exhibited a reproducible deposition of KCl(s) between each exposure, which makes possible the comparison between two experiments using this setup.

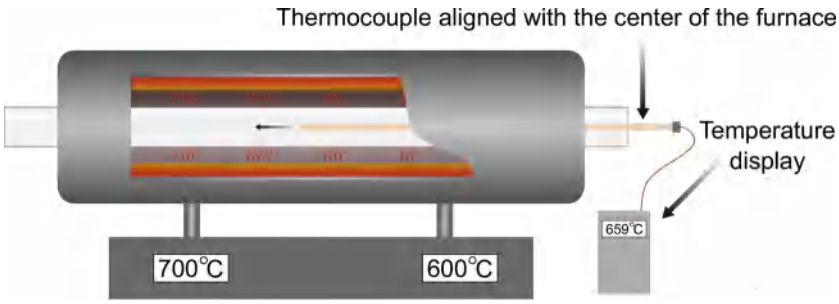

Fig. 3. Schematic drawing of the profile temperature measurements.

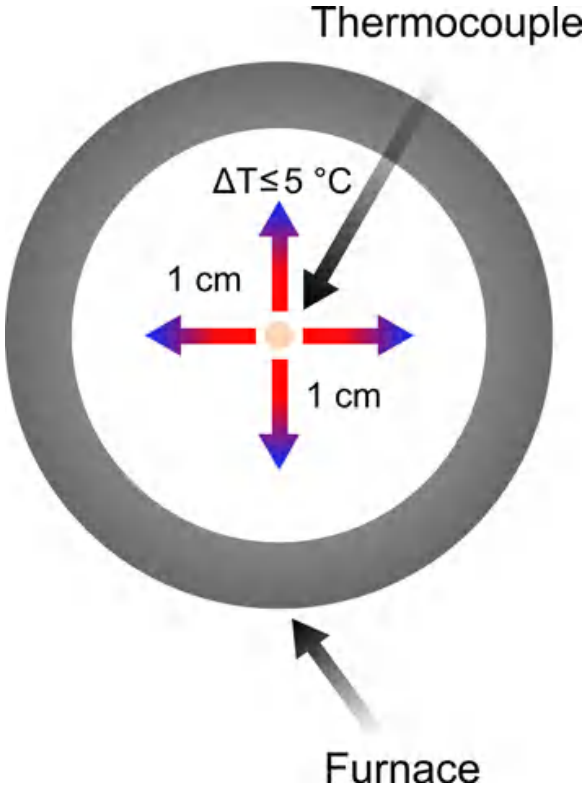

Fig. 5. Schematic drawing in a profile view of the temperature uncertainty observations.

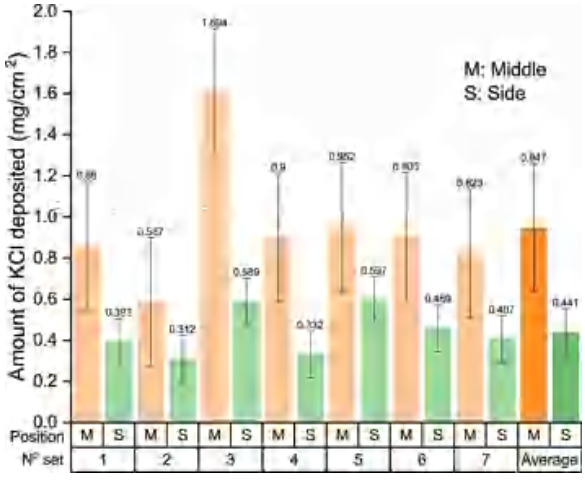

Fig. 6. Amount of KCl(s) deposited on gold foils every 24 h for one week at two samples position.

5.2. Characterization of the "low amount of KCl"-area

The optical inspection revealed no substantial deposition of KCl(s) for the "low amount of KCl"-area. These areas were usually located on the side of the samples facing the furnace wall. The lack of visual KCl was confirmed with the SEM/EDX analysis where the presence of KCl(s) on the sample surface was negligible (Fig. 8a). Despite the visual lack of KCl agglomerations on the sample's surface, the corrosion attack was severe already after 24 h of exposure in 5 % O_2 + 20 % H_2O at 600 °C under continuous KCl deposition.

Instead of present KCl particles, the sample surface was completely covered by an iron oxide, see Fig. 8a. The cross-sectional view in Fig. 8b confirms a two-layered oxide scale. Based on the EDX analysis

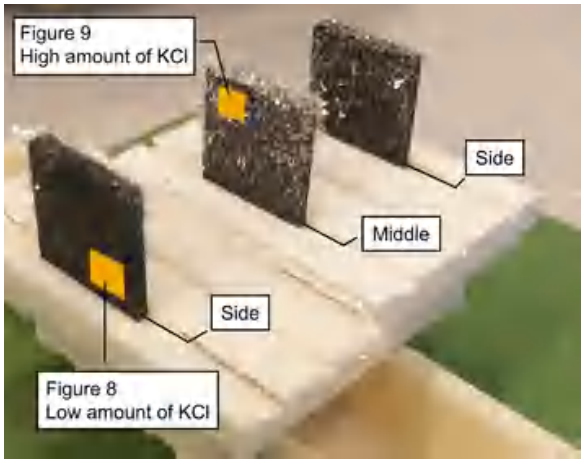

Fig. 7. Photograph of 304 L samples after an exposure for 24 h at 600 °C in 5 % O_2 + 20 %H_2O under continuous KCl deposition.

performed on this sample and earlier observation of 304 L exposed in the presence of small amounts of KCl(s) [21], the top oxide layer is suggested to be consisting of an outward-growing oxide of Fe_2O_3. Below this top oxide layer, an inward-growing oxide layer can be seen. This layer is suggested to be composed of fully oxidized, spinel oxide $(Fe,Cr,Ni)_3O_4$ as well as regions of mixed Fe,Cr spinel oxide and metal, again based on EDX analysis and earlier observations [21]. The thickness of the scale varies between 9 and 15 µm and no steel grain boundaries attack could be observed.

5.3. Characterization of the "high amount of KCl"-area

The areas with high amount of KCl were characterized by large agglomerations of deposited KCl(s). The largest crystals were removed gently by an air duster to make the sample preparation easier. A gradient of the spread of KCl could be observed during SEM/EDX analysis, which was shown by different surface topographies. Fig. 9 shows the plan view of a) the surface covered with KCl, b) a spalled area and c) the cross section of the area.

In Fig. 9a, the sample surface is completely covered by deposited KCl crystals. The cross-section was performed in this area and is shown in Fig. 9c. Shattered oxide layers beneath a continuous "crust" of KCl as well as steel grain boundaries attack are the observable features of this corrosion attack. The attack of grain boundaries reaches between 30 µm and 50 µm in depth. Another area where part of the corrosion product layer and the KCl deposit spalled off is shown in Fig. 9b. In this image, the steel grain boundaries attack was also evident.

SEM/EDX analysis of the cross-section shown in Fig. 9c is shown in Fig. 10. The corrosion products detected within the steel grain boundary attack is characterized as an oxide with the composition of O (53–56 %), Cr (18–21 %), Fe (15–19 %) and Ni (7–9 %) in at-%. Voids were observed along the grain boundaries and small amounts of chlorine were also detected within the steel grain boundaries.

6. Discussion

6.1. General observations

KCl in flue gas/deposit present in biomass- and waste-fired boilers is well known to cause an accelerated corrosion attack [2,33,34]. The corrosive effect of KCl has also been shown in several laboratory exposures [2,7,9–21,30–32]. However, comparing the extent of the corrosion attack of field exposed samples and laboratory exposed samples, the former is much more severe. This paper aims at, by increased corrosiveness in the laboratory exposures in a well-controlled manner, more closely resemble the corrosive environment of a biomass- and

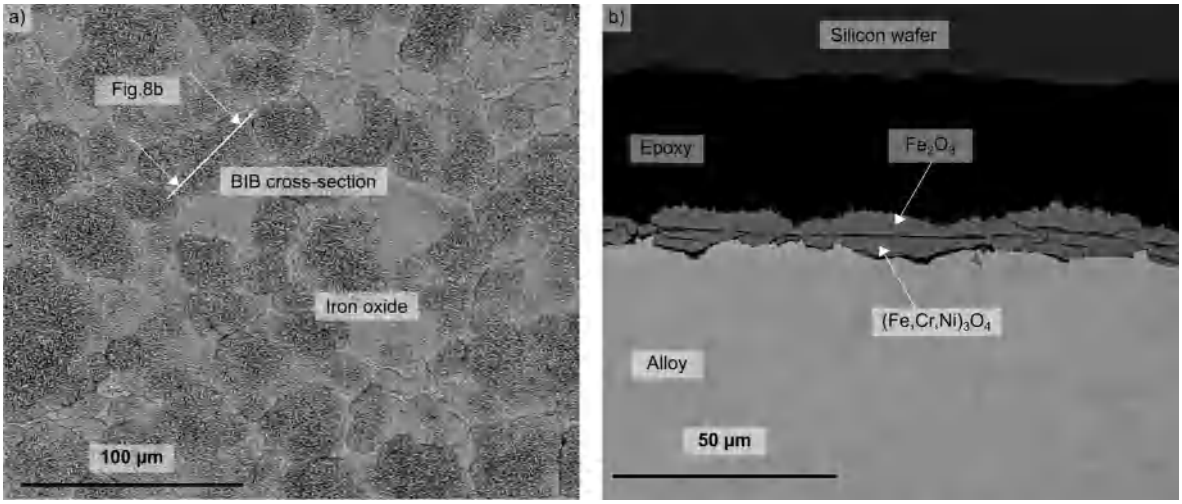

Fig. 8. SEM image using BSE of a) the plan view of a" low amount of KCl"-area of a 304 L sample after 24 h in 5 % O_2 + 20 % H_2O exposure under continuous KCl(s) deposition at 600 °C and b) a cross-sectional view.

waste-fired boiler. The reproducibility of this exposure setup with continuous deposition of KCl onto the samples is shown in Fig. 6. In order to make a reasonable comparison of the corrosion attack for both laboratory and field exposures, some parameters have been fixated. This study has selected the stainless steel 304 L as a reference material, the material temperature 600 °C and the exposure time 24 h.

6.2. *"Low amount of KCl"-area*

The features observed in this area are similar to 304 L samples exposed with 0.1 mg/cm^2 of KCl sprayed *ex-situ* prior to exposure (Fig. 11a). The morphology of the corrosion products of these KCl-sprayed samples is consistent with the observations mentioned in 5.2; an outward-growing Fe_2O_3 layer on top of an inward-growing spinel type oxide ($(Fe,Cr,Ni)_3O_4$) and regions of mixed Fe,Cr spinel oxide and metal [21]. The total thickness is usually between 7–9 µm and no signs of grain boundaries attack could be observed.

The features observed in the "low amount of KCl" areas are typical of KCl-induced corrosion on a stainless steel such as 304 L. The alkali reacts with the protective chromium-rich layer to form alkali chromates, *e.g.* potassium chromates in this study. This leads to depletion of chromium in the protective layer, resulting in less protective properties

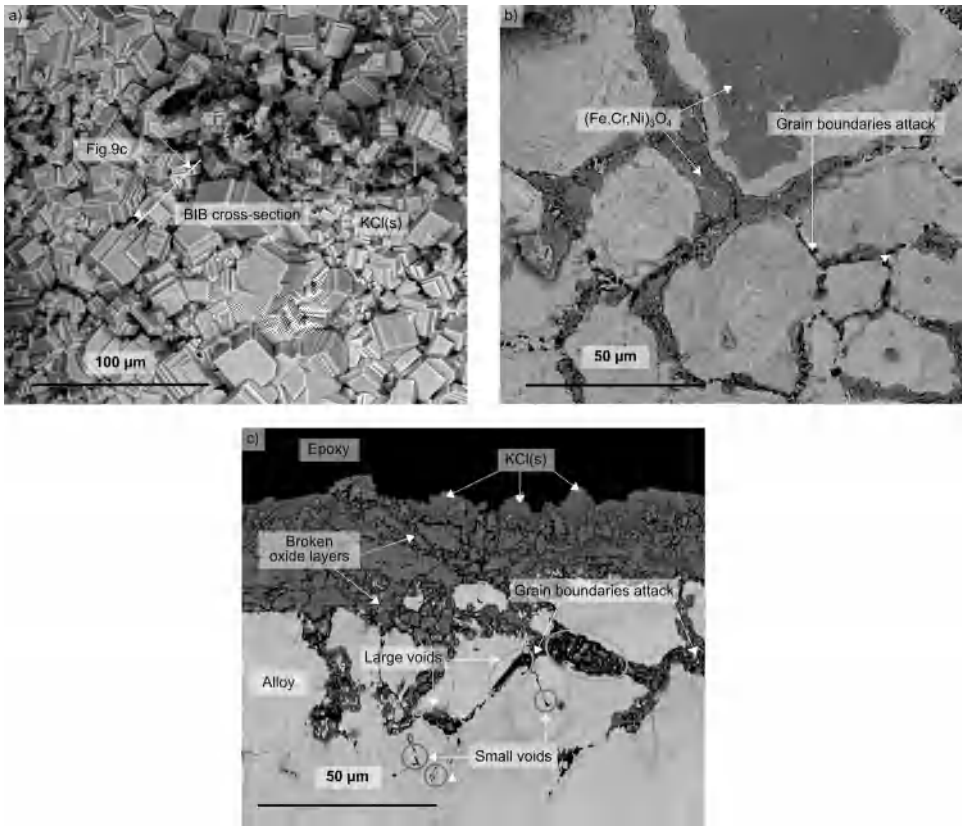

Fig. 9. SEM image using BSE for a) the plan view, b) a spalled area and c) a cross sectional view of a" high amount of KCl"-area after 24 h at 600 °C in 5 % O_2 + 20 % H_2O.

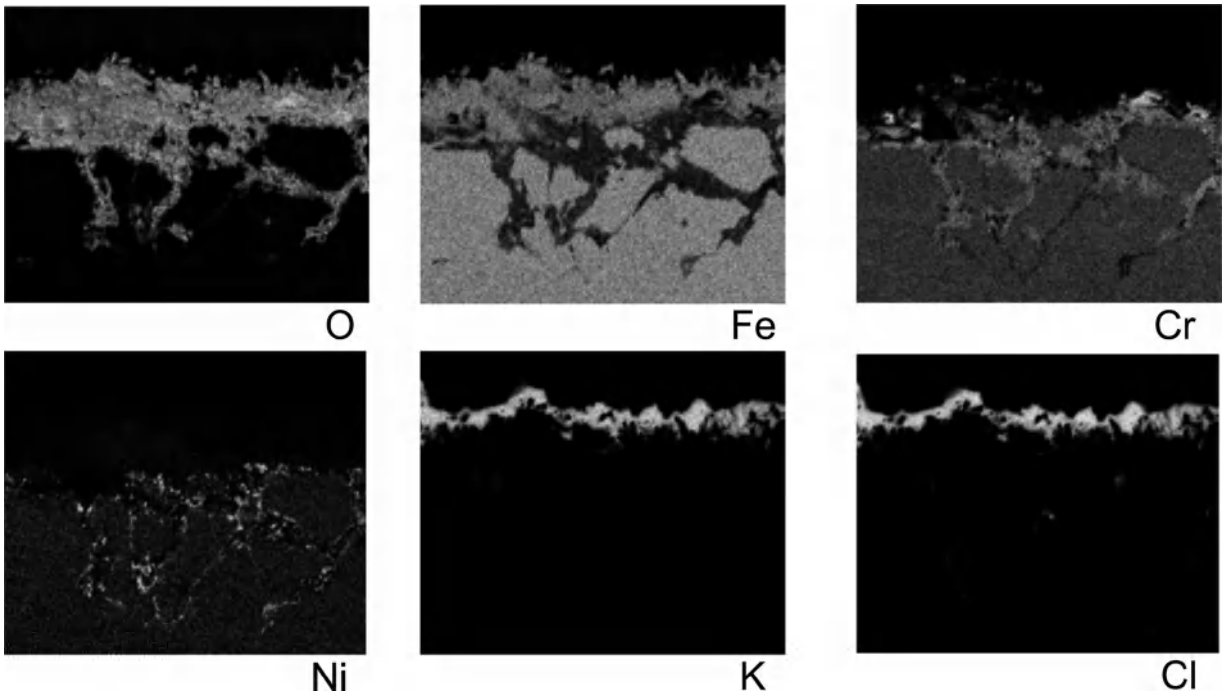

Fig. 10. EDX map of the cross section shown in Fig. 9c.

and ultimately, breakaway oxidation. In order to achieve this type of corrosion morphology, the alkali plays an important role and it have earlier been shown that *e.g.* K_2CO_3 (without any chlorine present) results in a similar corrosion attack [17].

This comparison between the two laboratory exposures methods mainly shows that the developed setup is able to reproduce an environment at least as corrosive as the KCl-spray method. The formation of alkali chromates followed by fast oxidation controlled by diffusion through the iron oxide is suggested to be the mechanism leading to the observable corrosion products. Therefore, it can be concluded that the setup is sufficiently efficient to create a corrosive environment in order to pursue further investigations.

6.3. "High amount of KCl"-area

This area shows the potential of the setup's abilities. The continuous deposition of KCl(s) and the simultaneous presence of KCl(g) during the exposure more closely simulates the complex environment in field, *e.g.* waste-fired boilers. Therefore, the aspect of corrosion products present in this area are more closely related to what can be observed on corresponding samples in field. Thick deposits (denoted as KCl "crust" in laboratory studies), together with thick and shattered oxide layers as well as deep steel grain boundary attack are the main characteristics.

According to the results, there is a correlation between the amount of KCl present on the surface of the sample and corrosiveness. At the "High amount of KCl"-area, the corrosion attack could be divided in two types; a general corrosion attack and steel grain boundary attack. For the "low amount of KCl"-area, the general corrosion attack was less severe compared to the "High amount of KCl"-area. Furthermore, the steel grain boundary attack was absent in the "low amount of KCl"-area. The steel grain boundary attack in the "High amount of KCl"-area showed signs of the presence of chlorine. This correlation is in agreement with Karlsson S et al. [30]. In the article referred to, 304 L was exposed in the presence of *ex-situ* added 0.1 mg/cm^2 and 1.0 mg/cm^2 of KCl, respectively, with and without SO_2 for 24 h at 600 °C. The extent of steel grain boundaries attacks increased with increased amount of available chlorine (either by increasing the amount of KCl (0.1 → 1.0 mg/cm^2 KCl or by introducing SO_2 and thereby releasing chlorine as HCl by the sulphation reaction of KCl). At most, the steel grain boundary attack reached 10 μm in depth [30]. As a comparison, in this

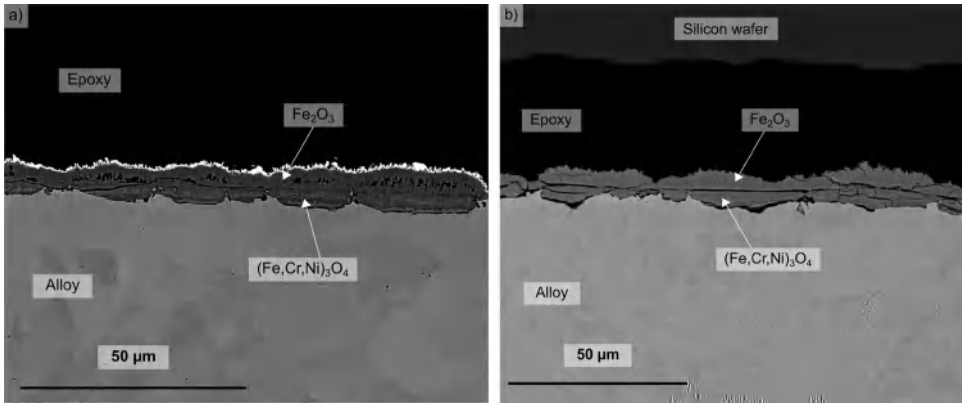

Fig. 11. SEM image using BSE of a cross section of a) 304 L sample exposed to 0.1 mg/cm^2 KCl(s) applied prior to exposure after 24 h at 600 °C in 5 % O_2 + 40 % H_2O [30] b) 304 L sample exposed to KCl(s) under continuous KCl(s) deposition after 24 h at 600 °C in 5 % O_2 + 20 % H_2O.

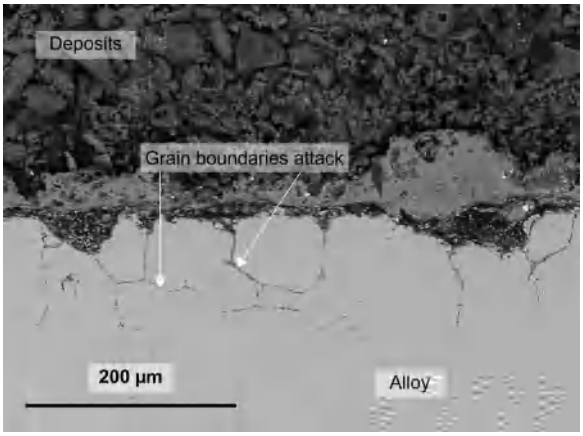

Fig. 12. SEM image using BSE of the cross section of a 304 L sample exposed for 24 h at 600 °C in a CFB boiler burning a waste mix (SRF + bark) [2].

study, the deposition rate of KCl shown in Fig. 6 indicates that in average, 0.95 mg/cm^2 of KCl is deposited every 24 h onto the middle sample, which is close to the 1,0 mg/cm^2 deposited in the referred article. Considering the heterogenous distribution of the KCl where most of the 0.95 mg/cm^2 of salt is located at the top of the sample, and the simultaneous presence of KCl in gaseous phase, a higher degree of overall corrosion was expected at the "high amount of KCl"-area. As previously mentioned in 5.3, the depth of the steel grain boundary attack reaches between 30 µm and 50 µm compared to 10 µm in the referred article. This indicates that the developed setup can create a more corrosive environment compared to the KCl-sprayed method.

This increase in the overall corrosion attack may be explained by the higher amount of potassium available, which would not only deplete the chromium from the protective oxide layer faster, thus, leading to breakaway oxidation in a shorter time. As a result, the amount of available chlorine is also expected to increase. However, the amount of chlorine detected in the corrosion attack is small. It is primarily detected at the corrosion front of the steel grain boundaries, as seen in Fig. 10. The exact role of chlorine at the corrosion front is still under debate and more work is required in order to understand the links between its presence and the corrosion attack.

According to the "Active oxidation"-mechanism [7,11,22–27] the chlorine is suggested to diffuse through the oxide scale as $Cl_2(g)$, reaching the oxide/metal interface and thereby forming corresponding metal chloride. The formed metal chloride is expected to volatilize and subsequently diffuse outward towards the oxide/environment interface. The metal chlorides then dissociate into metal oxide, releasing the chlorine gas, which may repeat the process or return to the atmosphere. However, in order for this cyclic process to work it is crucial that an oxygen gradient is preserved over the oxide scale, facilitating the formation of metal chlorides at the metal/oxide interface. It is unclear how the diffusion of $Cl_2(g)$ and the much larger $MeCl_x(g)$ is sustained through the oxide scale (or through voids, cracks and/or microcracks) whereas the diffusion of the much smaller $O_2(g)$ is not. Furthermore, the presence of $Cl_2(g)$ in a wet combustion atmosphere is expected to several orders of magnitude lower than $O_2(g)$.

Another approach to explain the diffusion of chlorine through the oxide scale is by the so-called electrochemical mechanism [25,29,36]. In this mechanism, the chloride ion Cl^- is suggested to diffuse along oxide grain boundaries towards the metal/oxide interface. As the chlorine ion is monovalent it is also suggested to diffuse faster compared to the divalent oxygen ion, resulting in an increased chlorine concentration at the metal/oxide interface. By decorating the oxide grain boundaries, the presence of chlorine is also suggested to increase the outward diffusion of metal ions.

Recent DFT work by Cantatore et al. [36] suggests that chlorine can also diffuse through bulk oxide using oxygen vacancies formed during oxidation. As such, the inward diffusion of chlorine is confined not only to oxide grain boundaries as suggested by [25,29]. However, no kinetic considerations have been applied. Hence, the main diffusive path of chlorine through the oxide scale, and as seen in this study, the steel grain boundaries, remains unclear.

Another feature observable in Fig. 9c is the presence of voids at the steel grain boundaries. The reasons behind the formation of large voids (green circles in Fig. 9c) are not yet fully understood. However, it may be due to the growth of oxide at the steel grain boundaries, inducing mechanical stresses which leads to displacements of steel grains. The large voids may also be due to the merging of smaller voids. Smaller voids can be observed (red circles in Fig. 9c) and might be the result of the diffusion of species leaving the area (i.e so called kirkendall effect). However, the mechanisms behind this void formation are still unclear and more work is needed in order to understand better these mechanisms.

One of the aims of this paper was to investigate a novel setup in order overcome the persisting difference in corrosion attack between laboratory and field exposures. Even if the developed setup mimics a more corrosive environment than previous methods [30–32], the corrosion attack remains not as severe as in a waste-fired boiler [2,34] (see *e.g.* Fig. 12 where the steel grain boundary attack reaches 140 µm). This difference could be explained by the more complex environment at the vicinity of superheaters. Temperature fluctuations, complex deposits accumulation and spallation, higher flow rate flue gas as well as complex flue gas chemistry may be the additional parameters which makes the corrosion attack in waste-fired boilers more severe.

The developed setup in this study offers new possibilities for studying KCl-induced corrosion phenomena in laboratory. As such, it was recently published a paper by Malede Yohanes C. et al., where the way of applying salt (applying a layer of KCl layer *ex-situ* prior to exposure compared to a continuous deposition) resulted in differences regarding the corrosion attack [37].

7. Conclusion

The scope of this paper was focused on a laboratory setup with continuous deposition of KCl(s) on 304 L samples at 600 °C. The results were compared to samples with KCl(s) sprayed *ex-situ* prior to exposure, as well as samples exposed in a waste-fired boiler. In the setup with continuous deposition of KCl(s) two areas could be distinguished: a "high amount of KCl"-area and a "low amount of KCl"-area. The analyses showed that the area with small amount of KCl(s) exhibited similar features to samples with 0.1 mg/cm^2 KCl(s) sprayed prior to exposure. The general corrosion morphology is characterized by an outward-growing Fe_2O_3 layer on top of an inward-growing spinel type oxide ($(Fe,Cr,Ni)_3O_4$) and regions of mixed Fe,Cr spinel oxide and metal as well as little or no signs of steel grain boundary attack. The corrosion attack was more severe in the "high amount of KCl"-areas, as steel grain boundary attack was triggered and reached a depth of 50 µm. This type of corrosion attack correlates well to previous results with samples with 1.0 mg/cm^2 KCl(s) sprayed prior to exposure, where grain boundary attacks were observed as well. However, the extent of the attack of the samples exposed to continuous deposition of KCl were much more severe. Compared to samples exposed in a waste-fired boiler, the grain boundary attack as well as the overall corrosion attack observed during continuous deposition of KCl are however still less severe.

Overall, this new laboratory method is able to create a more corrosive environment which more closely mimics the corrosion attack of samples exposed in full scale boilers as compared to the laboratory exposures where KCl(s) were applied *via ex-situ* spraying. The developed setup in this study may therefore offer new possibilities for future investigations of KCl-induced corrosion phenomena in a well-controlled manner. This emphasizes the relevance of using such methods in order to increase the knowledge in KCl-induced corrosion relevant for

biomass- and waste-fired boilers.

Data availability

The raw/processed data required to reproduce these findings cannot be shared at this time due to technical or time limitation.

CRediT authorship contribution statement

J. Phother-Simon: Conceptualization, Methodology, Validation, Investigation, Writing - original draft, Visualization. **T. Jonsson:** Conceptualization, Writing - review & editing, Supervision. **J. Liske:** Conceptualization, Writing - review & editing, Supervision.

Declaration of Competing Iinterest

The authors declare that they have no known competing financial interests or personal relationships that could have appeared to influence the work reported in this paper.

Acknowledgment

This work was carried out at the Swedish High Temperature Corrosion Centre (HTC) at Chalmers University of Technology and is hereby gratefully acknowledged together with its member companies (Sandvik Materials Technology, Sandvik Heating Technology, Energiforsk (represented by Vattenfall, E.ON Värme, Fortum Värme, Mälarenergi and Tekniska V. i Linköping) Valmet, Sumitomo SHI FW Energia Oy, Babcock & Wilcox Völund, Andritz, and Castolin). Financial support from Chalmers Area of Advance Energy is also acknowledged.

Appendix A. Supplementary data

Supplementary material related to this article can be found, in the online version, at doi:https://doi.org/10.1016/j.corsci.2020.108511.

References

[1] Available from: https://climate.nasa.gov/.
[2] S. Karlsson, L.-E. Åmand, J. Liske, Reducing high-temperature corrosion on high-alloyed stainless steel superheaters by co-combustion of municipal sewage sludge in a fluidised bed boiler, Fuel 139 (2015) 482–493.
[3] H. Kassman, L. Bäfver, L.-E. Åmand, The importance of SO2 and SO3 for sulphation of gaseous KCl – an experimental investigation in a biomass fired CFB boiler, Combust. Flame 157 (9) (2010) 1649–1657.
[4] H. Kassman, M. Broström, M. Berg, L.-E. Åmand, Measures to reduce chlorine in deposits: application in a large-scale circulating fluidised bed boiler firing biomass, Fuel 90 (4) (2011) 1325–1334.
[5] H. Kassman, J. Pettersson, B.-M. Steenari, L.-E. Åmand, Two strategies to reduce gaseous KCl and chlorine in deposits during biomass combustion—injection of ammonium sulphate and co-combustion with peat, Fuel Process. Technol. 105 (2013) 170–180.
[6] A.T. Masiá, B. Buhre, R. Gupta, T. Wall, Characterising ash of biomass and waste, Fuel Process. Technol. 88 (11–12) (2007) 1071–1081.
[7] H.P. Nielsen, F.J. Frandsen, K. Dam-Johansen, L.L. Baxter, The implications of chlorine-associated corrosion on the operation of biomass-fired boilers, Prog. Energy Combust. Sci. 26 (3) (2000) 283–298.
[8] S.V. Vassilev, D. Baxter, L.K. Andersen, C.G. Vassileva, T.J. Morgan, An overview of the organic and inorganic phase composition of biomass, Fuel 94 (2012) 1–33.
[9] K.O. Davidsson, L.-E. Åmand, B. Leckner, B. Kovacevik, M. Svane, M. Hagström, et al., Potassium, chlorine, and sulfur in ash, particles, deposits, and corrosion during wood combustion in a circulating fluidized-bed boiler, Energy Fuels 21 (1) (2007) 71–81.
[10] N. Folkeson, J. Pettersson, C. Pettersson, L.G. Johansson, E. Skog, B-Å Andersson, et al., Fireside corrosion of stainless and low alloyed steels in a waste-fired CFB boiler; the effect of adding sulphur to the fuel, Mater. Sci. Forum 595 (2008) 289–297. Trans Tech Publ.
[11] H.J. Grabke, E. Reese, M. Spiegel, The effects of chlorides, hydrogen chloride, and sulfur dioxide in the oxidation of steels below deposits, Corros. Sci. 37 (7) (1995) 1023–1043.
[12] S. Kiamehr, K.V. Dahl, M. Montgomery, M.A.J. Somers, KCl-induced high temperature corrosion of selected commercial alloys, Mater. Corros. 66 (12) (2015) 1414–1429.
[13] J. Lehmusto, P. Yrjas, Hupa M. Skrifvars BJ, High temperature corrosion of superheater steels by KCl and K2CO3 under dry and wet conditions, Fuel Process. Technol. 104 (2012) 253–264.
[14] S.C. Okoro, S. Kiamehr, M. Montgomery, F.J. Frandsen, K. Pantleon, Effect of flue gas composition on deposit induced high temperature corrosion under laboratory conditions mimicking biomass firing. Part I: exposures in oxidizing and chlorinating atmospheres, Mater. Corros. 68 (5) (2017) 499–514.
[15] S.C. Okoro, M. Montgomery, F.J. Frandsen, K. Pantleon, High temperature corrosion during biomass firing: improved understanding by depth resolved characterisation of corrosion products, Mater. High Temp. 32 (1–2) (2015) 92–101.
[16] J. Pettersson, H. Asteman, J.-E. Svensson, L.-G. Johansson, KCl induced corrosion of a 304-type austenitic stainless steel at 600°C; the role of potassium, Oxid. Met. 64 (1) (2005) 23–41.
[17] J. Pettersson, N. Folkeson, L.-G. Johansson, J.-E. Svensson, The effects of KCl, K2SO4 and K2CO3 on the high temperature corrosion of a 304-Type austenitic stainless steel, Oxid. Met. 76 (1) (2011) 93–109.
[18] J. Sui, J. Lehmusto, M. Bergelin, M. Hupa, The effects of KCl, NaCl and K2CO3 on the high-temperature oxidation onset of sanicro 28 steel, Oxid. Met. 85 (5) (2016) 565–598.
[19] H.P. Michelsen, F. Frandsen, K. Dam-Johansen, O.H. Larsen, Deposition and high temperature corrosion in a 10 MW straw fired boiler, Fuel Process. Technol. 54 (1) (1998) 95–108.
[20] M. Montgomery, A. Karlsson, In-situ corrosion investigation at Masnedø CHP plant–a straw-fired power plant, Mater. Corros. 50 (10) (1999) 579–584.
[21] T. Jonsson, S. Karlsson, H. Hooshyar, M. Sattari, J. Liske, J.-E. Svensson, et al., Oxidation after breakdown of the chromium-rich scale on stainless steels at high temperature: internal oxidation, Oxid. Met. 85 (5) (2016) 509–536.
[22] Y. Shinata, Accelerated oxidation rate of chromium induced by sodium chloride, Oxid. Met. 27 (5) (1987) 315–332.
[23] C.-J. Wang, T.-T. He, Morphological development of subscale formation in Fe–Cr–(Ni) alloys with chloride and sulfates coating, Oxid. Met. 58 (3) (2002) 415–437.
[24] J.M. Abels, H.H. Strehblow, A surface analytical approach to the high temperature chlorination behaviour of inconel 600 at 700 °C, Corros. Sci. 39 (1) (1997) 115–132.
[25] N. Folkeson, L.-G. Johansson, J.-E. Svensson, Initial stages of the HCl-induced high-temperature corrosion of alloy 310, J. Electrochem. Soc. 154 (9) (2007) C515–C521.
[26] M. McNallan, W. Liang, S. Kim, C. Kang, Acceleration of the high temperature oxidation of metals by chlorine, International Corrosion Conference Series, NACE, 1983.
[27] A. Zahs, M. Spiegel, H.J. Grabke, Chloridation and oxidation of iron, chromium, nickel and their alloys in chloridizing and oxidizing atmospheres at 400–700°C, Corros. Sci. 42 (6) (2000) 1093–1122.
[28] N. Folkeson, L.G. Johansson, J.E. Svensson, Initial stages of the HCl-Induced high-temperature corrosion of alloy 310, J. Electrochem. Soc. 154 (9) (2007) C515–C521.
[29] T. Jonsson, N. Folkeson, J.E. Svensson, L.G. Johansson, M. Halvarsson, An ESEM in situ investigation of initial stages of the KCl induced high temperature corrosion of a Fe–2.25Cr–1Mo steel at 400°C, Corros. Sci. 53 (6) (2011) 2233–2246.
[30] S. Karlsson, E. Larsson, T. Jonsson, J.-E. Svensson, J. Liske, A laboratory study of the in situ sulfation of alkali chloride rich deposits: corrosion perspective, Energy Fuels 30 (9) (2016) 7256–7267.
[31] S. Enestam, D. Bankiewicz, J. Tuiremo, K. Mäkelä, M. Hupa, Are NaCl and KCl equally corrosive on superheater materials of steam boilers? Fuel 104 (2013) 294–306.
[32] S.C. Okoro, M. Montgomery, F.J. Frandsen, K. Pantleon, Time and temperature effects on alkali chloride induced high temperature corrosion of superheaters during biomass firing, Energy Fuels 32 (7) (2018) 7991–7999.
[33] L. Mikkelsen, T. Jonsson, L. Paz, J. Eklund, J. Liske, B. Jonsson, et al., Increased steam temperature in grate fired boilers - Steamboost, KME 709 (2017) 113.
[34] P. Viklund, R. Pettersson, A. Hjörnhede, P. Henderson, P. Sjövall, Effect of sulphur containing additive on initial corrosion of superheater tubes in waste fired boiler, Corros. Eng. Sci. Technol. 44 (3) (2009) 234–240.
[35] C. Pettersson, T. Jonsson, C. Proff, M. Halvarsson, J.-E. Svensson, L.-G. Johansson, High temperature oxidation of the austenitic (35Fe27Cr31Ni) alloy sanicro 28 in O 2+ H 2 O environment, Oxid. Met. 74 (1-2) (2010) 93–111.
[36] V. Cantatore, M.A. Olivas Ogaz, J. Liske, T. Jonsson, J.-E. Svensson, L.-G. Johansson, et al., Oxidation driven permeation of Iron oxide scales by chloride from experiment guided first-principles modeling, J. Phys. Chem. C 123 (42) (2019) 25957–25966.
[37] Y.C. Malede, J.P. Simon, T. Jonsson, M. Montgomery, K.V. Dahl, J. Hald, KCl-induced corrosion of Ni-based alloys containing 35–45 wt % Cr, Mater. Corros. 70 (8) (2019) 1486–1506.